# Spin-transfer and fieldlike torques in antiferromagnets

Yuriy G. Semenov[1] and Ki Wook Kim[1,2,*]

[1]*Department of Electrical and Computer Engineering, North Carolina State University, Raleigh, North Carolina 27695, USA*
[2]*Department of Physics, North Carolina State University, Raleigh, North Carolina 27695, USA*

(Received 26 July 2021; accepted 21 October 2021; published 1 November 2021)

The phenomenon of spin-transfer torque (STT) in an antiferromagnet (AFM) is reexamined in terms of the incoming and outgoing spin currents. In contrast to the conventional approach, our model treats the STT as a result of the electron spin angular momentum transfer to the entire monodomain magnetic structure rather than to the individual sublattice magnetizations. This treatment enables the analysis to account for not only the destructive role of electron spin relaxation but also the potentially incomplete loss of electron spin phases that can either enhance the STT or suppress it depending on the structure parameters. Application of the developed model to the dynamical equation of the AFM order parameter illustrates the qualitative and quantitative differences with the conventional approach. Unlike the latter, our results predict a strong dependence of the STT on the orientation of the electron spin polarization relative to the magnetic anisotropy axes of the AFM. A similar characteristic also reveals a complex interplay in the Néel vector dynamics that can lead to a sublinear response of the oscillation frequency to the strength of the spin current. The impact of the fieldlike torque that can arise likewise from the spin injection is examined as well for a comprehensive account. The numerical calculations elucidate further the conditions that can elicit efficient manipulation of the magnetic states in an AFM under a spin-polarized current.

DOI: 10.1103/PhysRevB.104.174402

## I. INTRODUCTION

During the past two decades, the spin-transfer torque (STT) has been established as a highly reliable mechanism of magnetization switching in a ferromagnet (FM) under an electrical current [1]. The concept of STT supposes the recoil effect of spin-polarized electrons injected into a ferromagnetic layer [2,3]. Since the total angular momentum of the system (consisting of the electron spins and localized spin moments) remains unaltered under their exchange interaction, the change in the FM magnetization $\Delta M$ acquired during a (short) time period $\delta t$ is limited by the net spin angular momentum of $\delta N$ spin-polarized electrons incoming over the same duration (thus, $\frac{\hbar}{2}\delta N$). Accordingly, the resulting torque $\tau$ $(= \Delta\mathbf{M}/\delta t)$ is proportional to the electrical current $I$ $(= q_e\delta N/\delta t)$ through the FM layer (where $q_e$ denotes the electron charge). Taking into account that the exchange interaction with magnetic ions does not affect the electron spin component along the magnetization $\mathbf{M}$, the actual expression for the STT becomes [4]

$$\tau = \gamma\frac{\hbar}{2}\eta\frac{I}{V_{\mathrm{FM}}|q_e||\mathbf{M}|^2}\mathbf{M}\times(\mathbf{M}\times\mathbf{p}). \tag{1}$$

Here $\gamma$ is the gyromagnetic ratio, $V_{\mathrm{FM}}$ represents the volume of the free FM layer, and $\eta\mathbf{p}$ (with $\mathbf{p}$ defined as a unit vector) corresponds to the electron spin polarization $\mathbf{P}$ acquired in the adjacent hard FM with a fixed magnetization.

This widely used formula [Eq. (1)] implicitly assumes that the FM absorbs the transversal component $\mathbf{S}_\perp^{\mathrm{in}}$ of the incoming electron spin faster than the electron transit through the magnetic layer. On the other hand, the expression does not show any dependence on the strength of the carrier-ion exchange interaction. These shortcomings were addressed in part by the subsequent, more advanced treatments which explicitly accounted for the STT dependence on the finite penetration and precession lengths as well as the detrimental impact of spin relaxation [5–7]. The qualitative observation that the electrons exiting with a finite value in the transversal spin angular momentum $\mathbf{S}_\perp^{\mathrm{out}}$ can diminish or even amplify the recoil effect (i.e., the angular momentum transfer) depending on the sign of $\mathbf{S}_\perp^{\mathrm{in}}\cdot\mathbf{S}_\perp^{\mathrm{out}}$ suggests the importance of actual spin dynamics as the electrons move through the magnetic layer.

Spin dynamics becomes particularly significant for electrons traveling in an antiferromagnetic layer where the effect of a spin-polarized current is not so obvious. While the magnetization of an antiferromagnet (AFM) vanishes in the equilibrium ground state as it is well known, the rotation of the AFM order parameter (i.e., the Néel vector $\mathbf{L}$) generates a finite magnetization $\mathbf{M}$ proportional to the rate of its change. Accordingly, once $\mathbf{L}$ starts to move, it continues to rotate around $\mathbf{M}$ without any energy input or influence of the external magnetic fields until dissipation stabilizes the AFM in the ground state.

The conventional description of the STT in the AFMs presumes that the net impact of a spin current can be described by superposing the effects of individual spin densities $\mathbf{s}_A$ and $\mathbf{s}_B$ on AFM sublattices $A$ and $B$, in which the sublattices are treated as ferromagnetic compounds imbedded in an antiferromagnetic bulk (see, for instance, Refs. [8–10] and the references therein). A rigorous application of this treatment leads to the condition that the Néel vector is subject

*kwk@ncsu.edu

 

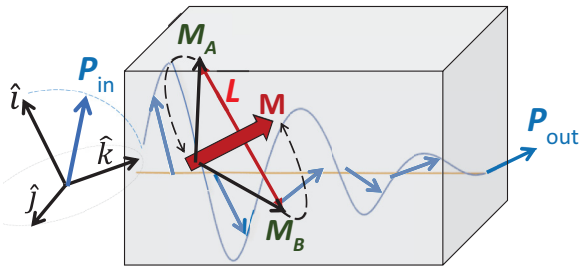


FIG. 1. Schematics of the spin-polarized electron dynamics injected into an AFM. The gray box represents the AFM, where sublattice magnetizations $\mathbf{M}_A$ and $\mathbf{M}_B$ form the Néel vector $\mathbf{L}$ and magnetization $\mathbf{M}$. The synchronous rotation of $\mathbf{M}_A$ and $\mathbf{M}_B$ around $\mathbf{M}$ is shown by the black dashed curves with arrows. Electron spins injected with polarization $\mathbf{P}_{\text{in}}$ precess around $\mathbf{M}$, while traveling through the AFM (blue arrows with the thin blue curve showing the trajectory). The instantaneous Cartesian coordinates $(\hat{\mathbf{i}}, \hat{\mathbf{j}}, \hat{\mathbf{k}})$ are defined such that $\hat{\mathbf{k}}$ aligns with $\mathbf{M}$ and $\hat{\mathbf{j}}$ is normal to the $\mathbf{M}$-$\mathbf{P}_{\text{in}}$ plane. A fraction of the difference in the incoming and outgoing momenta $\Delta\mathbf{P}$ $(= \mathbf{P}_{\text{in}} - \mathbf{P}_{\text{out}})$ is transmitted to the magnetization $\mathbf{M}$ triggering the STT; the rest is relaxed via the interaction with the AFM lattice, defects, etc.

to the staggered spin density $\delta\mathbf{s} = \mathbf{s}_A - \mathbf{s}_B = \xi\mathbf{n} \times \mathbf{s}$, where $\mathbf{n} = \mathbf{L}/|\mathbf{L}|$, $\mathbf{s} = \mathbf{s}_A + \mathbf{s}_B$, and $\xi$ is the ratio between the spin precession time around the magnetic moment of one sublattice and the time the carriers spend in this sublattice. Consequently, the carrier-ion exchange interaction induces the STT $\tau \sim \mathbf{n} \times \delta\mathbf{s}$ whose expression resembles the torque on a FM [Eq. (1)] but with the coefficient in front redefined to account for $\xi$. As such, the quantitative result requires an accurate analysis of electron spin dynamics related to each sublattice to estimate parameter $\xi$—a rather challenging problem. At the same time, the shortcomings of the conventional STT model discussed earlier in relation to the FMs also apply similarly. Of those, electron spin relaxation may be especially important in the AFMs with compensated exchange fields of sublattices. Manipulation of the AFM states by a spin-polarized current has become a subject of intense study due, in part, to the anticipated advantages in the operating speed and energy efficiency over the FM counterparts [11].

In the present work we reexamine the theoretical description of the STT in the AFMs based on a higher-level phenomenology in place of the individual sublattice responses to the spin-polarized current. More specifically, the angular momentum conservation attributed to the carrier-ion exchange interaction is applied to only two variables, i.e., the net AFM magnetization and the spin moments of the incoming electrons as illustrated schematically in Fig. 1. Such a treatment allows a universal description of electron spin momentum transfer not limited by the particular manner of the magnetic structure response including, for instance, the creation/annihilation of thermal magnons [12], electron reflection at the AFM/FM junctions [5], electron spin drift-diffusion [6], or diffusive transport [7]. In doing so, only the spin evolution during the electron exposure becomes the subject of analysis in terms of the phenomenological relaxation parameters involved in the Bloch equations. The resulting imitative recoil effect drives the AFM order parameter. To simplify the problem, an adiabatic approximation is used that assumes a short electron transit time in the quasistable (or quasistatic) AFM magnetic texture. Application to a monodomain free layer reveals that this model can lead to the results quantitatively and qualitatively different from the conventional treatment, while the two also converge when the underlying assumptions for the latter are satisfied. The impact of the fieldlike torque that can arise similarly from the spin injection is also examined for a comprehensive analysis.

## II. THEORETICAL MODEL

### A. Electron spin dephasing and relaxation

The Néel vector response to a spin-polarized electrical current can be analyzed in an approach similar to the STT in a FM layer. The main assumption is the adiabatic approximation that can effectively separate the fast electron spin dynamics (i.e., the ultrashort electron transit time) and the relatively slow response of AFM sublattice magnetization. The evolution of the electron spin $\mathbf{S}$ in a quasistatic magnetic field $\mathbf{B} = \mathbf{b}|\mathbf{B}|$ is adequately accounted for by the Bloch equations [13]

$$\frac{d\mathbf{S}}{dt} = \gamma\mathbf{S} \times \mathbf{B} - \frac{\mathbf{b}[\mathbf{S} \cdot \mathbf{b} - S_0(\mathbf{B})]}{T_1} - \frac{\mathbf{b} \times (\mathbf{S} \times \mathbf{b})}{T_2}. \quad (2)$$

Here the second and third terms describe the relaxation of spin components longitudinal and transversal to the magnetic field with the characteristic time constants $T_1$ and $T_2$, respectively; $\mathbf{b}S_0(\mathbf{B})$ denotes the equilibrium state corresponding to the effective field $\mathbf{B}$ of the given instant. Note that the *decoherence* of the electron spin considered in Eq. (2) originates from its interaction (i.e., the loss of angular momentum) with the crystal lattice rather than the magnetic texture. When an ensemble of electron spins is involved as in the present case, additional sources of the relaxation need to be accounted for. For instance, the randomness in the carrier trajectories inside the AFM layer evidently leads to a variation in their transit times, resulting in the complete or partial loss of transversal spin correlation in the course of precession around the exchange field $\mathbf{B}$ and scattering on the defects, AFM imperfections, and spin fluctuations. These effects can also be incorporated into the Bloch equation by adding the *dephasing* rate $1/T^*$ to the third term via an effective transversal relaxation time $T_2^* = (1/T_2 + 1/T^*)^{-1}$. Considering the dependence of $T^*$ on $B$ (i.e., the strength of the exchange interaction), it is reasonable to expect that $T_2^*$ is dominated by $T_2$ as $B \to 0$. Due to its nontrivial dependence on the details of carrier dynamics, this parameter $(T^*)$ is treated as a phenomenological constant for simplicity.

To solve Eq. (2) explicitly, it is convenient to introduce the Cartesian coordinate system with unit vector $\hat{\mathbf{k}}$ pinned to the direction of the exchange field $\mathbf{b}$, $\hat{\mathbf{i}}$ perpendicular to $\mathbf{b}$ on the $(\mathbf{b}, \mathbf{p})$ plane, and $\hat{\mathbf{j}}$ normal to the $(\mathbf{b}, \mathbf{p})$ plane, i.e.,

$$\hat{\mathbf{i}} = \frac{\mathbf{p} - \mathbf{b}(\mathbf{p} \cdot \mathbf{b})}{\sqrt{1 - (\mathbf{p} \cdot \mathbf{b})^2}} = \frac{\mathbf{b} \times (\mathbf{p} \times \mathbf{b})}{\sqrt{1 - (\mathbf{p} \cdot \mathbf{b})^2}},$$
$$\hat{\mathbf{j}} = \frac{\mathbf{b} \times \mathbf{p}}{\sqrt{1 - (\mathbf{p} \cdot \mathbf{b})^2}}, \quad \hat{\mathbf{k}} = \mathbf{b}. \quad (3)$$

As defined above, $\mathbf{p}$ corresponds to the direction of injected electron spin polarization (thus, parallel to the *fixed* FM layer

magnetization). Then the solution of Eq. (2) under a quasistatic effective field $\mathbf{B}$ takes a simple form of $\mathbf{S}(t) = \hat{\mathbf{i}}S_i + \hat{\mathbf{j}}S_j + \hat{\mathbf{k}}S_k$:

$$\begin{aligned} S_i(t) &= S_\perp(0)e^{-t/T_2^*}\cos\gamma Bt, \\ S_j(t) &= -S_\perp(0)e^{-t/T_2^*}\sin\gamma Bt, \\ S_k(t) &= S_\parallel(0)e^{-t/T_1} + S_0(B)[1-e^{-t/T_1}]. \end{aligned} \tag{4}$$

Here $S_\perp(0)$ and $S_\parallel(0)$ denote the electron spin components transversal and longitudinal to $\mathbf{B}$ at time $t = 0$ (i.e., when entering the free AFM layer). This expression for $\mathbf{S}(t)$ can be further specified by considering the conditions of the incoming spin-polarized electrons. Assuming that $\delta N$ electrons are injected into the AFM over time $\delta t$ with a spin-polarization efficiency or fraction $\eta$, we obtain $S_\parallel(0) = \frac{\hbar}{2}\eta\delta N(\mathbf{p}\cdot\mathbf{b})$ and $S_\perp(0) = \frac{\hbar}{2}\eta\delta N\sqrt{1-(\mathbf{p}\cdot\mathbf{b})^2}$.

As for the effective field $\mathbf{B}$ that dictates the electron spin precession, the net AFM magnetization is the appropriate choice for the exchange field that acts on the conducting electrons. The electrons, on average, experience the mutual action of the localized spin moment ensemble belonging to both AFM sublattices in the layer. Accordingly, we can express it as

$$\mathbf{B} = \frac{\mathbf{M}}{M_\Sigma}\frac{J_{\rm ex}}{\gamma\hbar}. \tag{5}$$

The constant $J_{\rm ex}$ of the carrier-ion exchange interaction corresponds to the conduction-band spin splitting presuming a virtual ferromagnetic alignment of AFM sublattice magnetizations $\mathbf{M}_s$ in the same direction. In the bipartite AFMs, the total magnitude of collinear sublattice magnetizations becomes $M_\Sigma = 2M_s$. Following Eq. (5), unit vector $\mathbf{b}$ can be further defined as $\mathbf{M}/|\mathbf{M}|$.

With the obtained $\mathbf{S}(t)$, the torque induced by the spin-polarized electrons can be calculated. Electron spins, while traversing the AFM layer, dispense $\Delta\mathbf{S} = \mathbf{S}(0) - \mathbf{S}(t_{\rm dr})$ of their polarization through spin relaxation and dephasing processes as discussed earlier. In other words, $\delta N$ electrons can exit the AFM layer with a finite amount of nonequilibrium angular moment [i.e., $\mathbf{S}(t_{\rm dr})$] unlike the treatment in the conventional approach. Moreover, the AFM angular moment experiences the recoil effect only from the transversal spin component $\Delta\mathbf{S}^* = \Delta\mathbf{S} - \mathbf{b}(\mathbf{b}\cdot\Delta\mathbf{S})$ as the longitudinal part commutes with the former. Of $\Delta\mathbf{S}^*$, a fraction is transferred to the AFM net angular moment via the carrier-ion exchange interaction ($\sim\frac{T_2}{T_2+T^*}$), while the rest is lost to the lattice through the spin-orbital and nonsecular part of the spin-spin interaction ($\sim\frac{T^*}{T_2+T^*}$). If the injected electrons precess several times around $\mathbf{B}$ during the stay in the AFM layer, they induce a torque $\sim\frac{T_2}{T_2+T^*}\frac{\Delta\mathbf{S}^*}{\delta t}$ [4], i.e.,

$$\begin{aligned} \tau(\mathbf{b}) = \frac{T_2}{T_2+T^*}\frac{\gamma\hbar\eta j}{2L_{\rm AFM}|q_e|} \\ \times[\mathbf{b}\times(\mathbf{p}\times\mathbf{b})(1-e^{-t_{\rm dr}/T_2^*}\cos\gamma Bt_{\rm dr}) \\ +(\mathbf{b}\times\mathbf{p})e^{-t_{\rm dr}/T_2^*}\sin\gamma Bt_{\rm dr}], \end{aligned} \tag{6}$$

where $j$ is the current density through the AFM and $L_{\rm AFM}$ denotes the corresponding layer thickness.

In the limit of short dephasing time $T^* \ll t_{\rm dr}, T_2$ (thus $T_2^* \approx T^*$), Eq. (6) reproduces the well-known result of the STT in a FM metal [i.e., Eq. (1) with $\mathbf{b}$ replaced by the normalized FM magnetization $\mathbf{M}/|\mathbf{M}|$]. In the opposite case of a relatively long dephasing time $T_2^* \gtrsim t_{\rm dr}$, the result suggests that the torque can increase up to a factor of 2 at $\gamma Bt_{\rm dr} \simeq (2k-1)\pi$ or be suppressed to a small value when $\gamma Bt_{\rm dr} \simeq 2\pi k$, $k = 1, 2, \ldots$. Equation (6) also shows the self-evident dependence of the effective torque on the carrier-ion exchange, leading to $\tau(\mathbf{b}) \to 0$ through vanishing $B$ and $1/T^*$. Similarly, $\tau(\mathbf{b})$ tends to zero in the limit of extremely short transit time $t_{\rm dr} \to 0$ where the electron spins cannot affect the magnet structure.

### B. Application to AFM dynamical equations

To incorporate the torque $\tau(\mathbf{b})$ into the dynamical equation for the AFM order parameter, the magnetization needs to be expressed in terms of this order parameter. In the common case of an AFM with collinear magnetizations $\mathbf{M}_A$ and $\mathbf{M}_B$ of two sublattices $A$ and $B$ ($\mathbf{M}_B = -\mathbf{M}_A$ in the equilibrium state), the order parameter becomes the Néel vector $\mathbf{L} = \mathbf{M}_A - \mathbf{M}_B$ while magnetization is $\mathbf{M} = \mathbf{M}_A + \mathbf{M}_B$. To proceed further, it is convenient to introduce dimensionless $\mathbf{n} = \mathbf{L}/2M_s$ and $\mathbf{m} = \mathbf{M}/2M_s$. This leads to $|\mathbf{m}| \ll |\mathbf{n}| \approx 1$ when the system does not deviate significantly from equilibrium. Using the dimensionless variables and Newton's notation $\dot{\mathbf{n}} \equiv \frac{d}{dt}\mathbf{n}$, the magnetization takes the form [8]

$$\mathbf{m} = \frac{1}{2\omega_{\rm ex}}\dot{\mathbf{n}}\times\mathbf{n} + \frac{\gamma\mathbf{H}_0}{2\omega_{\rm ex}}, \tag{7}$$

where $\omega_{\rm ex} = \gamma H_{\rm ex}$ with the exchange field $H_{\rm ex}$ that establishes antiferromagnetic correlations between sublattices $A$ and $B$. The carrier spin components longitudinal to the instantaneous direction of the AFM magnetization mediate an exchange field $\mathbf{H}_0$ ($\parallel \mathbf{m}$) at both sublattices, i.e.,

$$\mathbf{H}_0 = \mathbf{b}(\mathbf{p}\cdot\mathbf{b})\frac{\eta_z J_{\rm ex}\Omega n_e}{\gamma\hbar} = \frac{\mathbf{m}(\mathbf{p}\cdot\mathbf{m})}{m^2}\frac{\eta_z J_{\rm ex}\Omega n_e}{\gamma\hbar}, \tag{8}$$

where $\eta_z$ is the spin polarization averaged over electron trajectories in a monodomain AFM with the primitive cell volume $\Omega$ and concentration $n_e$ of the injected electrons. The injected electron density $n_e$ can be expressed further as $\frac{\delta N}{V_{\rm AFM}}\frac{t_{\rm dr}}{\delta t}$.

Combining Eqs. (7) and (8), we can express $\mathbf{m}$ via $\mathbf{n}$,

$$\mathbf{m} = \frac{(\dot{\mathbf{n}}\times\mathbf{n})}{2\omega_{\rm ex}}\left[1 + \frac{\eta_z J_{\rm ex}\Omega n_e}{\hbar}\frac{\mathbf{p}\cdot(\dot{\mathbf{n}}\times\mathbf{n})}{|\dot{\mathbf{n}}\times\mathbf{n}|^2}\right]. \tag{9}$$

This equation also explicitly defines the magnetization direction $\mathbf{b} = (\dot{\mathbf{n}}\times\mathbf{n})/|\dot{\mathbf{n}}\times\mathbf{n}|$ as a function of the AFM vector $\mathbf{n}$. Substituting these expressions into Eq. (6) leads to the effective torque in terms only of the Néel vector:

$$\begin{aligned} \tau(\mathbf{n}) = \frac{T_2}{T_2+T^*}\frac{\eta\gamma\hbar j}{2L_{\rm AFM}|q_e|}\left[\left(\mathbf{p} - \dot{\mathbf{n}}\times\mathbf{n}\,\frac{\mathbf{p}\cdot(\dot{\mathbf{n}}\times\mathbf{n})}{|\dot{\mathbf{n}}\times\mathbf{n}|^2}\right)\right. \\ \times(1-e^{-t_{\rm dr}/T_2^*}\cos\gamma Bt_{\rm dr}) \\ \left.+\frac{\mathbf{n}(\dot{\mathbf{n}}\cdot\mathbf{p}) - \dot{\mathbf{n}}(\mathbf{n}\cdot\mathbf{p})}{|\dot{\mathbf{n}}\times\mathbf{n}|}e^{-t_{\rm dr}/T_2^*}\sin\gamma Bt_{\rm dr}\right], \end{aligned} \tag{10}$$

where the strength of the carrier-ion exchange field becomes

$$B = m\frac{J_{\rm ex}}{\gamma\hbar} = \frac{J_{\rm ex}|\dot{\mathbf{n}}\times\mathbf{n}|}{2\omega_{\rm ex}\gamma\hbar}\left[1+\frac{\eta_z J_{\rm ex}\Omega n_e}{\hbar}\frac{\mathbf{p}\cdot(\dot{\mathbf{n}}\times\mathbf{n})}{|\dot{\mathbf{n}}\times\mathbf{n}|^2}\right]. \quad (11)$$

Equation (11) clearly reveals that the phase of the outgoing spin polarization $\gamma B t_{\rm dr}$ not only depends on $t_{\rm dr}$ but also changes, in contrast to a FM, with the evolution of the Néel vector.

Note that the conventional approach to the STT supposes a simpler expression $\mathbf{p}-\mathbf{n}(\mathbf{p}\cdot\mathbf{n})$ in place of those in the square bracket of Eq. (10) along with the trivial prefactor $\frac{T_2}{T_2+T^*}=1$, i.e.,

$$\tau_0(\mathbf{n}) = \frac{\eta\gamma\hbar j}{2L_{\rm AFM}|q_e|}[\mathbf{p}-\mathbf{n}(\mathbf{p}\cdot\mathbf{n})]. \quad (12)$$

In this description, the exchange fields originating from the respective sublattice magnetizations $\mathbf{M}_A, \mathbf{M}_B$ (thus, $\parallel \mathbf{n}$ approximately) affect the electron spin dynamics individually rather than the effective field from the net magnetization $\mathbf{M}$ ($\parallel \mathbf{m}$) of the AFM. It also fails to consider the dependence of the STT on the strength of carrier-ion exchange interaction, resulting in a finite STT in the limit $J_{\rm ex}\to 0$. In comparison, the vanishing $\tau(\mathbf{n})$ in Eq. (10) is ascertained by zero $B$ ($\propto J_{\rm ex}$) which leads to the absence of spin precession and subsequently dephasing ($1/T^*\to 0$) as discussed briefly above. More importantly, the simple model predicts the strongest STT effect when the injected spins polarize perpendicular to the Néel vector (i.e., $\mathbf{p}\cdot\mathbf{n}=0$). In this configuration, however, $\mathbf{p}$ can actually become collinear to the AFM magnetization $\mathbf{m}$ ($\propto \dot{\mathbf{n}}\times\mathbf{n}$) that excludes electron spin precession around it. The consequence is the failure of spin transfer to the AFM, which evidently contravenes the prediction of the earlier approach, while it is fully consistent with the current treatment [i.e., Eq. (10)]. Additional discussions on this and other particularities of the phenomenology developed above are provided in Sec. III.

Along with the STT, $\mathbf{H}_0$ given in Eq. (13) can also contribute to the Néel vector dynamics. Considering that the electrons partially lose the longitudinal polarization with the relaxation rate $1/T_1$ while traversing the AFM layer, the effective field can be written in terms of $\mathbf{n}$ as

$$\mathbf{H}_0 = \left[\frac{T_1}{t_{\rm dr}}(1-e^{-t_{\rm dr}/T_1})\eta\right]\frac{n_e J_{\rm ex}\Omega_0}{\gamma\hbar}\frac{\mathbf{p}\cdot(\dot{\mathbf{n}}\times\mathbf{n})}{|\dot{\mathbf{n}}\times\mathbf{n}|^2}(\dot{\mathbf{n}}\times\mathbf{n}). \quad (13)$$

Here the expression given in the square brackets actually corresponds to the mean value $\eta_z$ of spin polarization used in Eq. (8). Once the relevant parameters become known, the STT and fieldlike torque (via $\mathbf{H}_0$) can be incorporated into the dynamical equation for the AFMs for numerical solutions.

### C. AFM dynamics under spin-transfer and fieldlike torques

As stated, both the STT and the fieldlike torque mediated by the exchange field affect the AFM magnetization $\mathbf{m}$. Since this is a variable auxiliary to the Néel vector $\mathbf{n}$, it can be eliminated from the set of expressions starting with the Landau-Lifshitz-Gilbert equation for each sublattice. Following the condition $|\mathbf{m}|\ll|\mathbf{n}|$ and the identity $\mathbf{H}_0\cdot\mathbf{n}=0$, the final equation of the Néel vector motion subject to the spin-transfer and fieldlike torques reads [14]

$$\left[\ddot{\mathbf{n}}+\omega_r^2\frac{\partial}{\partial\mathbf{n}}\frac{W(\mathbf{n})}{K_a}+2\delta_r\dot{\mathbf{n}}\right]\times\mathbf{n}+\gamma\dot{\mathbf{H}}_0+2\omega_{\rm ex}\frac{\tau(\mathbf{n})}{M_s}=0, \quad (14)$$

where $W(\mathbf{n})$ is the density of anisotropy energy and $\delta_r$ is the half-width of the AFM resonance. It is not surprising that $\tau(\mathbf{n})$ induces an acceleration in the Néel vector (i.e., the second time derivative) rather than its rotation (i.e., the first time derivative, which is the case for a FM). This difference stems from the dynamical nature of AFM magnetization vanishing at a stationary Néel vector [see, for instance, Eq. (9)].

To proceed further, it is convenient to establish the dimensionless time $t\to\omega_r t$ in terms of the frequency $\omega_r$ of zero-field AFM resonance. This characteristic frequency is given as $\omega_r=\gamma\sqrt{2H_{\rm ex}H_a}$, where the effective anisotropy field $H_a=K_a/M_s$ is specified by the anisotropy constant $K_a$. Introducing the dimensionless anisotropy energy density $w(\mathbf{n})=W(\mathbf{n})/K_a$ and dimensionless magnetic field $\mathbf{h}=\gamma\mathbf{H}_0/\omega_r$, Eq. (14) takes the canonical form

$$\left[\ddot{\mathbf{n}}+\frac{\partial w(\mathbf{n})}{\partial\mathbf{n}}+2\frac{\delta_r}{\omega_r}\dot{\mathbf{n}}\right]\times\mathbf{n}+\tau_{\rm ST}=-\dot{\mathbf{h}}, \quad (15)$$

where the spin torque in the dimensionless units becomes

$$\tau_{\rm ST}=\frac{\tau(\mathbf{n})}{M_s\omega_r}\sqrt{\frac{2H_{\rm ex}}{H_a}}. \quad (16)$$

The contribution of the longitudinal exchange field (i.e., the fieldlike torque) appears in Eqs. (14) and (15) as a time derivative of $\mathbf{H}_0$. As such, the field effect is expected to be negligible compared with the STT in a steady-state mode of operation established after the damping of transient processes. On the other hand, applying an input current pulse with a steep leading edge (e.g., $\omega_r t_r\ll 1$ with the characteristic rise time $t_r$) can make the term $\dot{\mathbf{h}}$ sufficiently strong to cause the Néel vector motion in the course of *transient* processes. In an ideal condition, this term can take the form of a $\delta$ function, i.e., $\dot{\mathbf{h}}=\mathbf{p}h_0\delta(t)$, where $h_0=\eta n_e J_{\rm ex}\Omega_0/\omega_r\hbar$ is the pulse amplitude. The impetus at $t=0$ can set the Néel vector into rotation which, with the aid of the characteristic inertial motion, can lead to the switching into a desired energy minimum [15]. Nevertheless, the practically achievable concentration of the injected spin-polarized electrons is limited in the current-driven case and, thus, can mediate only a relatively slow Néel vector rotation (compared to $\omega_r$). Furthermore, the configuration most suitable for the fieldlike torque (e.g., $\mathbf{p}$ parallel to the AFM hard axis) is highly undesirable for the STT. In the general case of an arbitrary $\mathbf{p}$ direction, the fieldlike torque just determines the initial conditions from which the Néel vector evolves via the STT. Even this [thus, the $\dot{\mathbf{h}}$ term in Eq. (15)] can be ignored conveniently when the asymptotic AFM behavior at $t\to\infty$ is the focus of the analysis, since the initial conditions do not influence the final state.

## III. RESULTS AND DISCUSSION

For further analysis, it is necessary to specify the properties of the structure under consideration. As it is typical among the metallic AFMs, the free AFM layer is assumed to have an easy plane (say, $x$-$y$) with an additional preference in one

of the in-plane directions resulting in an easy axis (e.g., $x$). Such coexistence of easy and hard axes can be described by the anisotropy energy density

$$W = \tfrac{1}{2}\left(K_x n_x^2 + K_z n_z^2\right), \tag{17}$$

where $K_z > 0$ and $K_x < 0$ set the hard-$z$ and easy-$x$ axes, respectively. Accordingly, $|K_x|$ corresponds to the anisotropy constant $K_a$ defined earlier (thus, the anisotropy field $H_a = |K_x|/M_s$). Considering the normalization condition $|\mathbf{n}| = 1$, it is convenient to adopt the polar-coordinate representation $\mathbf{n} = (\sin\theta\cos\varphi, \sin\theta\sin\varphi, \cos\theta)$ with the polar $\theta = \theta(t)$ and azimuthal $\varphi = \varphi(t)$ angles. Then Eq. (15) can be rewritten in terms of $\theta$ and $\varphi$ in two coupled equations as

$$\begin{aligned}\ddot{\theta} = {} & \tfrac{1}{2}\sin 2\theta(\dot{\varphi}^2 + \kappa_z - \kappa_x\cos^2\varphi) \\ & - 2\lambda\dot{\theta} - (\dot{h}_x\sin\varphi - \dot{h}_y\cos\varphi) - \tau_\theta\end{aligned} \tag{18}$$

and

$$\ddot{\varphi} = \frac{\kappa_x}{2}\sin 2\varphi - 2\cot\theta\dot{\theta}\dot{\varphi} - 2\lambda\dot{\varphi} + \csc^2\theta(\dot{h}_z + \tau_\varphi), \tag{19}$$

where $\lambda = \delta_r/\omega_r$, $\kappa_z = K_z/|K_x|$, and $\kappa_x = K_x/|K_x|$. The terms $\tau_\theta$ and $\tau_\varphi$ for the STT become rather complex functions of angular variables. To solve Eqs. (18) and (19), the initial conditions on $\theta$, $\varphi$, $\dot{\theta}$, and $\dot{\varphi}$ are needed. Here the equilibrium position of $\theta = \pi/2$ and $\varphi = 0$ (i.e., along the easy $x$ axis) is used as the initial state, while the initial velocities in angular variables $\dot{\varphi}(0)$ and $\dot{\theta}(0)$ are determined by the leading edge of the driving current applied at $t = 0$ as discussed earlier. By assuming an abrupt turn-on (thus a $\delta$ function for $\dot{\mathbf{h}}$), Eq. (15) gives $\dot{\varphi}(0) = p_z h_0$ and $\dot{\theta}(0) = p_y h_0$.

It is instructive to compare the evolution of the Néel vector in terms of our [Eq. (10)] and conventional STT approaches with the incoming spin polarization $\mathbf{p}$ oriented along the hard $z$ axis. In this configuration, the electron spins may transfer their angular momenta as much as $\mathbf{p}$ deviates from the direction of the net AFM magnetic moment $\mathbf{m}$ ($\perp \mathbf{n}$). As the Néel vector $\mathbf{n}$ (thus, sublattice magnetizations $\mathbf{M}_A$ and $\mathbf{M}_B$) starts to rotate on the $x$-$y$ plane [e.g., $\theta(0) = \pi/2$ and $\dot{\theta}(0) = 0$ with $p_y = 0$ as given above], $\mathbf{m}$ is aligned along the $z$ axis normal to the $x$-$y$ plane [15]. This minimizes the spin components transversal to $\mathbf{m}$ and excludes the effect of STT from the Néel vector dynamics, which is the case in our model (see also the discussion in Sec. II B). The conventional treatment, in contrast, considers the individual sublattice torques whose sum does not vanish under an electric current with the spins polarized along the hard axis. This qualitative difference can be readily verified in the experiments.

The picture given above is further validated by the analysis of $\tau_\theta$ and $\tau_\varphi$ in the limiting case. When $T^* \to 0$ (i.e., rapid spin dephasing analogous to the commonly adopted treatment), the STT terms for $\mathbf{p} \parallel \hat{\mathbf{z}}$ yield

$$\tau_\theta = \frac{\eta\gamma\hbar j\omega_{\rm ex}}{L_{\rm AFM}|q_e|M_s\omega_r}\frac{\dot{\theta}\dot{\varphi}\sin^2\theta}{\sin^2\theta\dot{\varphi}^2 + \dot{\theta}^2}, \tag{20}$$

$$\tau_\varphi = \frac{\eta\gamma\hbar j\omega_{\rm ex}}{L_{\rm AFM}|q_e|M_s\omega_r}\left(1 - \frac{\dot{\varphi}^2\sin^4\theta}{\dot{\varphi}^2\sin^2\theta + \dot{\theta}^2}\right). \tag{21}$$

As expected, the torque evidently becomes zero for the strong anisotropy of the hard $z$ axis which dictates the equilibrium initial position of the Néel vector at $\theta = \pi/2$ and $\dot{\theta} = 0$. Needless to say, the STT becomes nonzero in general for an arbitrary direction of the electron spin polarization.

In the numerical solution of Eqs. (18) and (19), the values typical for metallic AFMs are assumed for the material parameters as follows [10,16]: $T_2 = 10$ ps, $T_1 = 20$ ps, $\eta = 0.4$, $L_{\rm AFM} = 6$ nm, $\Omega_0 = 0.05$ nm$^3$, $J_{\rm ex} = 1$ eV, $K_x = -3\times10^4$ erg/cm$^3$, $K_z = 1.5\times10^5$ erg/cm$^3$, $\omega_r = 10^{12}$ s$^{-1}$, $M_s = 4\pi\times 110$ G, and $\lambda = 0.1$. Estimation of the electron density $n_e$ is achieved by using the data for IrMn of $\rho = 8.6\times10^{-5}$ $\Omega$ cm and electron mobility 50 cm$^2$/V s [17]. This set of parameters ensures the applicability of the model for the range of the electrical current $j \sim 10^7$–$10^8$ A/cm$^2$ provided that the electron transit time in the AFM layer is shorter than the inverse of the resonant frequency, i.e., $t_{\rm dr}\omega_r \ll 1$. On the other hand, each electron spin can still rotate multiple times over the duration $t_{\rm dr}$ around the strong exchange field of polarized sublattices (i.e., the carrier-ion exchange interaction). Since the actual strength of the AFM magnetization evolves with the Néel vector dynamics, the electron spin rotation is also a variable in time. As such, a comparison of the conditions for Néel vector reversal can provide a crucial example in highlighting the difference between the current and conventional approaches. For simplicity of the analysis, it is convenient to take $T^*$ to be much shorter than $t_{\rm dr}$ as it eliminates the potential effects of spin relaxation which can complicate the picture. This is what we adopt hereinafter.

Figure 2 highlights the drastic discrepancy between the two treatments. As qualitatively discussed above, our approach indeed reveals a strong dependence on the electron spin orientation relative to the AFM magnetization $\mathbf{m}$, which is clearly visible in Fig. 2(a). With the current density fixed at a sufficient large value of $6\times10^7$ A/cm$^2$, the injected electron spin polarization set along the $+z$ hard axis [$\psi = 0^\circ$; thus, $\mathbf{p} \parallel \mathbf{m}(\perp \mathbf{n})$] fails to induce any change in the Néel vector as anticipated, while the case of $\psi = 45^\circ$ (i.e., $\mathbf{p} \nparallel \mathbf{m}$) rotates it successfully by 180° ($n_x = +1 \to n_x = -1$). By contrast, the calculations based on the conventional model result in the efficient Néel vector reversal for both orientations (not shown). It is also noted that the existing model tends to predict a lower current density for the operation than our approach. As can be seen from Fig. 2(b), $j = 10^7$ A/cm$^2$ is apparently strong enough to cause the Néel vector flip in the former but not in the latter even for $\psi = 45^\circ$.

Since the orientation of $\mathbf{p}$ becomes an important factor for the efficient manipulation of the Néel vector (and also a clearly distinguishing feature of the current model), its impact on the Néel vector reversal is further examined. Figure 3 plots the ranges of polar and azimuthal angles $(\psi, \phi)$ of $\mathbf{p}$ at which the current pulse (of a fixed strength and optimally matched duration) results in the Néel vector reversal. As shown, the STT appears to be the most efficient at around 45° on the $x$-$z$ plane (i.e., the easy and hard axes, respectively). The allowed range of reversal obviously increases with the driving current density.

The calculation results discussed thus far suppose a short dephasing time $T^*$ compared to the transit time $t_{\rm dr}$ as mentioned earlier. For a more comprehensive understanding, we also examine the impact of the spin relaxation/dephasing on the STT by relaxing this condition. Our numerical investigation indicates that the $T_2^*/t_{\rm dr}$ ratio does not affect the Néel vector dynamics significantly once it becomes $\lesssim$0.4.

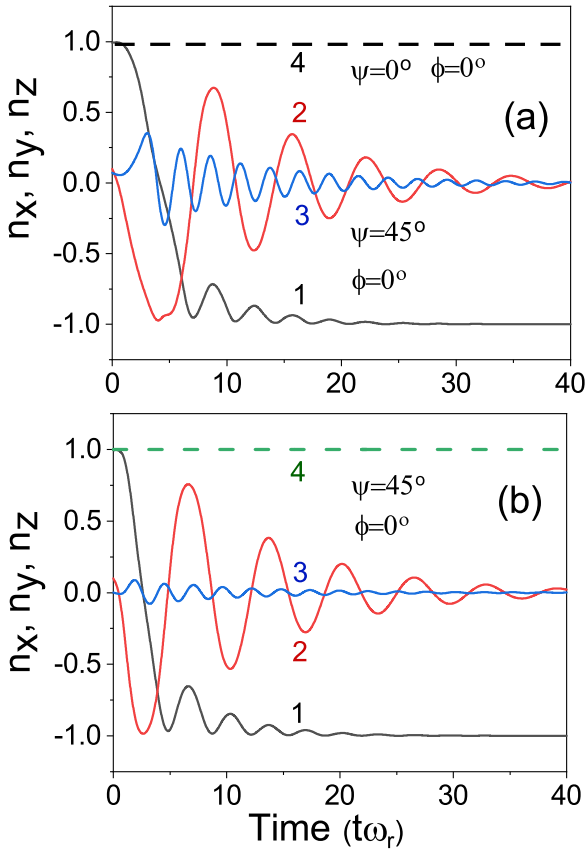


FIG. 2. (a) Temporal evolution of the STT induced Néel vector $\mathbf{n}(t)$ dynamics calculated by our model for two different orientations of electron spin polarization. The current density $j$ of $6 \times 10^7$ A/cm$^2$ is assumed with the pulse duration of 3 ps. The polarization orientation is varied from the hard $z$ axis toward the easy $x$ axis in the $x$-$z$ plane (thus, the azimuthal angle $\phi$ fixed at 0° with the polar angle $\psi$ varying). Curves 1, 2, 3 correspond to the $x$, $y$, $z$ components of the Néel vector for the case of $\psi = 45°$, while curve 4 (dashed line) shows only the $x$ component (i.e., $n_x$) for $\psi = 0°$. The straight line for curve 4 (i.e., $\psi = 0°$) indicates no change in $\mathbf{n}(t)$ despite the applied STT. In contrast, curves 1, 2, 3 (i.e., $\psi = 45°$) illustrate the Néel vector reversal. (b) Comparison of the Néel vector response between the conventional and our models at a lower current density of $10^7$ A/cm$^2$ (pulse duration ~1 ps) and spin polarization of $\psi = 45°$, $\phi = 0°$. Curves 1, 2, 3 denote $n_x$, $n_y$, $n_z$ obtained from the conventional model, demonstrating the Néel vector reversal. By comparison, curve 4 showing $n_x$ from our model indicates no rotation. In both (a) and (b) the dephasing time is assumed to be much shorter than the electron transit time.

As $T_2^*/t_{dr}$ increases above this value (for instance, by decreasing $t_{dr}$), the result unexpectedly does not reproduce the alternating strength of the STT despite the oscillatory term (i.e., $\cos \gamma B t_{dr}$), which is unlike the case of the FM free layer discussed earlier in Sec. II A. As it turns out, the phase oscillations in the effective field $B$ are intricately dependent on the Néel vector evolution according to Eq. (11). A careful analysis shows that the STT actually becomes suppressed once $T_2^*/t_{dr} > 0.4$, further highlighting the difference with the conventional model (which provides no such dependence). Accordingly, it is indeed crucial to ensure rapid dephasing of

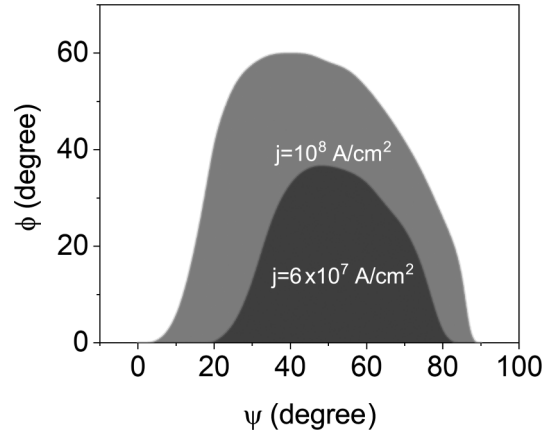


FIG. 3. Range of injected electron spin polarization orientations enabling the Néel vector reversal for two different values of the current density (shaded regions in the polar $\psi$ and azimuthal $\phi$ angle representation). The dephasing time is assumed to be much shorter than the electron transit time as in Fig. 2.

the injected electron spin polarization. Likewise, extending $t_{dr}$ may be similarly beneficial (e.g., by controlling the sample length and quality); however, this route is also limited by $\omega_r^{-1}$.

Along with the switching, another interesting phenomenon associated with the STT is the excitation of steady Néel

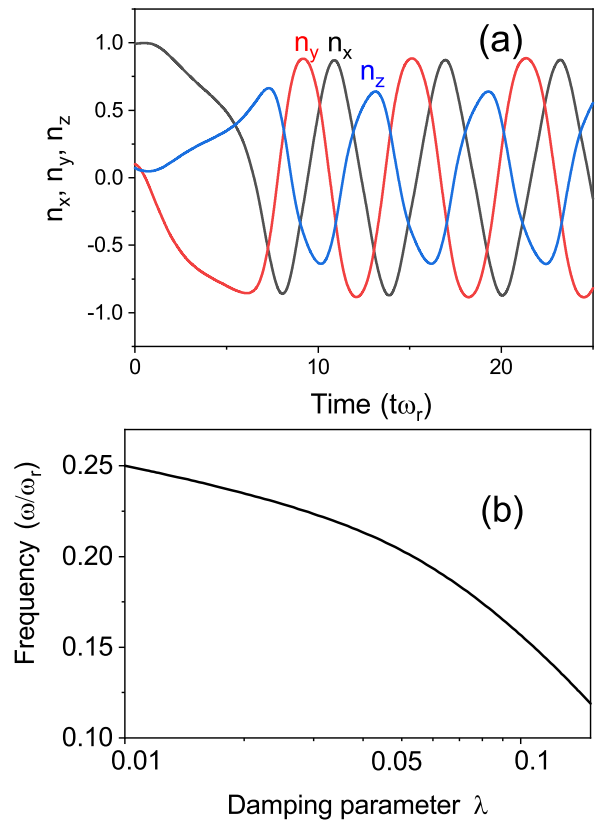


FIG. 4. (a) Excitation of steady Néel vector oscillations by the STT with the electron spin polarization $\psi = 45°$, $\phi = 0°$, current density $j = 6.5 \times 10^7$ A/cm$^2$, and damping parameter $\lambda = 0.1$. (b) Néel vector oscillation frequency as a function of $\lambda$. The conditions for $\mathbf{p}$ and $j$ are the same as in (a).

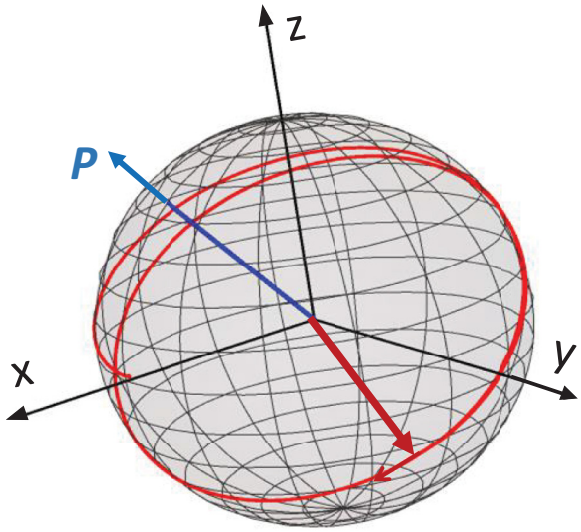


FIG. 5. Trajectory of Néel vector oscillation on the Bloch sphere starting from the easy $x$ axis for the time span of 0–15 ps (red curve). The blue and red arrows denote the electron spin polarization **P** and the Néel vector **n**, respectively. The driving conditions are the same as in Fig. 4(a).

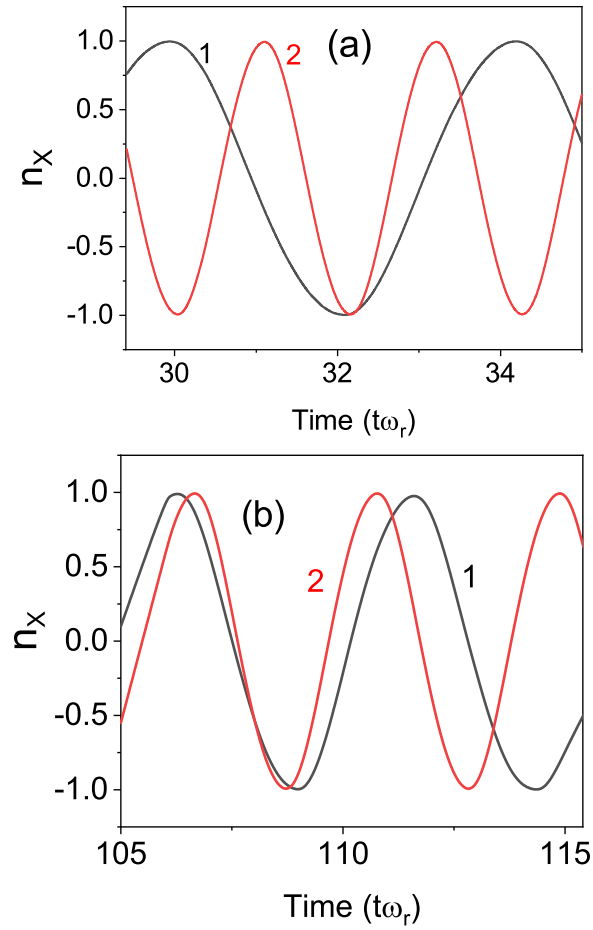


FIG. 6. $x$ component of the Néel vector demonstrating the STT-induced steady oscillations following the initial transient phase in a uniaxial AFM. A hard $z$ axis with the anisotropy constant $K_z = 1.5 \times 10^5$ erg/cm$^3$ (as in other figures) is assumed along with an easy $x$-$y$ plane. (a) The comparison is between $j = 10^6$ A/cm$^2$ (curve 1) and $j = 2 \times 10^6$ A/cm$^2$ (curve 2), while $T^*\omega_r$ is fixed at 0.1. (b) The dephasing time $T^*\omega_r$ is varied (0.1 and 0.3 for curves 1 and 2, respectively) with $j = 10^6$ A/cm$^2$. For both (a) and (b), the electron spin polarization $\psi = 45^\circ$, $\phi = 0^\circ$ and the damping parameter $\lambda = 0.1$ are used.

vector oscillations. In an AFM with biaxial anisotropy, the oscillations appear if the spin current mediates an antidamping torque that exceeds the damping characterized by the parameter $\lambda$ $(= \delta_r/\omega_r)$ and anisotropy potential barrier in Eqs. (18) and (19). The approach developed above indeed reveals the possibility to generate the Néel vector oscillations with a driving current above a certain threshold value. Figure 4(a) illustrates the Néel vector oscillations following the initial transient phase ($t\omega_r < 10$) under the current density $j = 6.5 \times 10^7$ A/cm$^2$ and electron spin polarization $\mathbf{p} = (45^\circ, 0^\circ)$. The steady precession around **p** appears to have the Néel vector nearly lying on a plane normal to the rotation axis as plotted in Fig. 5. The threshold value for the onset of oscillations is estimated to be $\approx 6 \times 10^7$ A/cm$^2$. As $j$ increases, the transient dynamics become shorter but the oscillation frequency $\omega$ shows only a weak dependence.

In comparison, the conventional model predicts a more significant influence of the driving current density on $\omega$. The reason for this difference lies in the fact that the net AFM magnetization **m** is entirely mediated by the spin-polarized current which actually draws the relatively small **m** closer to the polarization **P** as the current density goes up. Such a reorientation tends to suppress the STT as discussed above (i.e., the decrease in the transversal component). By contrast, the individual sublattice magnetization (i.e., AFM) or the magnetization of a FM reveals intrinsic, inherent characteristics whose magnitudes are hardly affected by the external influence (thus, little/no impact on the torque applied to each sublattice). This also explains why the calculations based on the conventional approach predict the threshold current density significantly smaller at $\sim 10^7$ A/cm$^2$ along with higher oscillation frequencies. A similar argument applies to the reversal described above as well [i.e., Fig. 2(b)]. The comparison clearly suggests that the earlier model may have overestimated the effectiveness of the current-driven STT in the AFMs. At the same time, our approach shows that the oscillation frequency can be controlled more sensitively by the damping parameter $\lambda$ [Fig. 4(b)].

Actually, the configuration more amenable for the steady Néel vector oscillations is the uniaxial easy-plane AFMs, where the axial symmetry may support the helical wave formation under a small local torque [18]. In the case of a monodomain structure, this uniaxial symmetry merely corresponds to the absence of the easy-axis anisotropy in Eq. (17), i.e., keeping the hard $z$ axis with $K_z > 0$ while setting $K_x = 0$. The result shown in Fig. 6(a) clearly indicates the generation of steady Néel vector oscillations even with a small current density $j = 10^6$ A/cm$^2$ and electron spin polarization $\mathbf{p} = (45^\circ, 0^\circ)$ as the STT does not need to overcome the anisotropy barrier in the easy $x$-$y$ plane. Moreover, the oscillation frequency reveals a direct dependence on $j$, which can be seen from the comparison between the cases with $j = 10^6$

and $2 \times 10^6$ A/cm$^2$. The current densities involved appear to be too small to reorient sufficiently the magnetization **m** toward the spin polarization **p** to induce the suppression of the STT discussed earlier. We also examine the influence of the dephasing time on the torque [Fig. 6(b)]. Surprisingly, a relatively longer dephasing time (i.e., $T^*\omega_r = 0.3$) appears to enhance the STT (thus, the higher oscillation frequency) unlike the biaxial case. Such characteristics of the Néel vector dynamics cannot be described by the conventional model.

These and other properties of the STT predicted by our model for the AFMs illustrate the need for a validation with the measurements. However, experimental studies to-date on the magnetization switching in the AFMs have focused almost exclusively on the spin-orbit torques including the so-called Néel spin-orbit torque (see, for a recent work, Ref. [19] as well as the references therein). Very recently, an investigation was reported on the STT-driven Néel vector dynamics in AFM PtMn and IrMn [20]. While the structure adopted in this measurement closely resembled the example considered here, the necessary short spin current pulse was generated by the ultrafast demagnetization of the optically excited FM layer and subsequent spin diffusion instead of the usual bias-driven spin-polarized electrical current. Furthermore, the detection was via the magneto-optical Kerr effect, where the static Kerr rotation signal was unknown [20]. The resulting gaps in the knowledge render a direct comparison with the modeling results (from both the conventional and our approaches) yet to be achieved. Further inquiry is called for.

## IV. SUMMARY

A theoretical model for the STT is developed based on a phenomenological treatment of the total angular momentum conservation in a magnetic structure between the injected carrier spins and the localized magnetic ion spins that constitute the magnetization **M**. The electron spin dynamics $\mathbf{S}(t)$ is described by the Bloch equation in a quasistatic exchange field approximation since the electron transit through a nanoscale magnetic layer is generally much faster than the relatively slow response of **M**. The damping of the injected spins including the dephasing due to the dispersion of electron paths can be accounted for via the characteristic time constants. The resulting **S** as a function of time $t$ enables us to obtain the desired net angular momentum transfer to the magnetic layer as the difference between incoming and outgoing electron spin momenta. The developed model is applied to the dynamical equation of the AFM order parameter under a spin-polarized electrical current for a comprehensive description. The numerical solutions indicate a significant deviation from the predictions of the conventional approach in a number of aspects. The physical origin appears to be the discrepancy in the treatment of the exchange field with which the injected electron spins interact; namely, the AFM magnetization **M** (our model) vs the sublattice magnetizations $\mathbf{M}_A$, $\mathbf{M}_B$ (the conventional approach). The fact that the AFM magnetization is entirely mediated by the spin-polarized current further introduces a complex interplay in the Néel vector dynamics. Considering both qualitative and quantitative differences in the characteristic features, it is anticipated that the accuracy of the developed model can be assessed rather straightforwardly through experimental studies.

## ACKNOWLEDGMENT

This work was supported, in part, by the U.S. Army Research Office (W911NF-20-2-0166).

[1] D. C. Ralph and M. D. Stiles, Spin transfer torques, J. Magn. Magn. Mater. **320**, 1190 (2008).
[2] J. C. Slonczewski, Current-driven excitation of magnetic multilayers, J. Magn. Magn. Mater. **159**, L1 (1996).
[3] L. Berger, Emission of spin waves by a magnetic multilayer traversed by a current, Phys. Rev. B **54**, 9353 (1996).
[4] Y. G. Semenov and K. W. Kim, Modeling of antiferromagnetic dynamics: A brief review, IEEE Nanotechnol. Mag. **14**, 32 (2020).
[5] Y. Tserkovnyak, A. Brataas, G. E. W. Bauer, and B. I. Halperin, Nonlocal magnetization dynamics in ferromagnetic heterostructures, Rev. Mod. Phys. **77**, 1375 (2005).
[6] C. Petitjean, D. Luc, and X. Waintal, Unified Drift-Diffusion Theory for Transverse Spin Currents in Spin Valves, Domain Walls, and Other Textured Magnets, Phys. Rev. Lett. **109**, 117204 (2012).
[7] P. Baláž, J. Barnaś, and J.-P. Ansermet, Transverse spin penetration length in metallic spin valves, J. Appl. Phys. **113**, 193905 (2013).
[8] H. V. Gomonay and V. M. Loktev, Spin transfer and current-induced switching in antiferromagnets, Phys. Rev. B **81**, 144427 (2010).
[9] A. McDonald and M. Tsoi, Antiferromagnetic metal spintronics, Philos. Trans. R. Soc. London Sect. A **369**, 3098 (2011).
[10] V. Baltz, A. Manchon, M. Tsoi, T. Moriyama, T. Ono, and Y. Tserkovnyak, Antiferromagnetic spintronics, Rev. Mod. Phys. **90**, 015005 (2018).
[11] E. V. Gomonay and V. M. Loktev, Spintronics of antiferromagnetic systems, Low Temp. Phys. **40**, 17 (2014).
[12] X. G. Wang, Y.-Z. Nie, L. Chotorlishvili, Q. L. Xia, J. Berakdar, and G. H. Guo, Electron-magnon spin conversion and magnonic spin pumping in an antiferromagnet/heavy metal heterostructure, Phys. Rev. B **103**, 064404 (2021).
[13] A. Abragam, *The Principles of Nuclear Magnetism* (Clarendon, Oxford, 1961), Chap. 1.
[14] A. F. Andreev and V. I. Marchenko, Symmetry and the macroscopic dynamics of magnetic materials, Sov. Phys. Usp. **23**, 21 (1980).
[15] Y. G. Semenov and K. W. Kim, Spin pumping torque in antiferromagnets, Appl. Phys. Lett. **110**, 192405 (2017).
[16] R. Khymyn, I. Lisenkov, V. Tiberkevich, B. A. Ivanov, and A. Slavin, Antiferromagnetic THz-frequency Josephson-like oscillator driven by spin current, Sci. Rep. **7**, 43705 (2017).
[17] J. Zhou, X. Wang, Y. H. Liu, J. H. Yu, H. X. Fu, L. Liu, S. H. Chen, J. Y. Deng, W. N. Lin, X. Y. Shu, H. Y. Yoong, T. Hong, M. Matsuda, P. Yang, S. Adams, B. H. Yan, X. F. Han, and J. S.

Chen, Large spin-orbit torque efficiency enhanced by magnetic structure of collinear antiferromagnet IrMn, Sci. Adv. **5**, 6696 (2019).

[18] Y. G. Semenov, X.-L. Li, X. Xu, and K. W. Kim, Helical waves in easy-plane antiferromagnets, Phys. Rev. B **96**, 224432 (2017).

[19] S. Arpaci, V. Lopez-Dominguez, J. Shi, L. Sánchez-Tejerina, F. Garesci, C. Wang, X. Yan, V. K. Sangwan, M. A. Grayson, M. C. Hersam, G. Finocchio, and P. K. Amiri, Observation of current-induced switching in noncollinear antiferromagnetic $IrMn_3$ by differential voltage measurements, Nat. Commun. **12**, 3828 (2021).

[20] K. Kang, W.-B. Lee, D.-K. Lee, K.-J. Lee, and G.-M. Choi, Magnetization dynamics of antiferromagnetic metals of PtMn and IrMn driven by a pulsed spin-transfer torque, Appl. Phys. Lett. **118**, 252407 (2021).